Journal of *Marine Science and Engineering*

MDPI

Article

Relative Sea-Level Rise Projections and Flooding Scenarios for 2150 CE for the Island of Ustica (Southern Tyrrhenian Sea, Italy)

Marco Anzidei [1], Daniele Trippanera [1,*], Alessandro Bosman [2,3], Franco Foresta Martin [1,4], Fawzi Doumaz [1], Antonio Vecchio [5,6], Enrico Serpelloni [1], Tommaso Alberti [1], Sante Francesco Rende [3] and Michele Greco [7]

1 Istituto Nazionale di Geofisica e Vulcanologia, 00143 Rome, Italy; marco.anzidei@ingv.it (M.A.); sidereus@rocketmail.com (F.F.M.); fawzi.doumaz@ingv.it (F.D.); enrico.serpelloni@ingv.it (E.S.); tommaso.alberti@ingv.it (T.A.)
2 Istituto di Geologia Ambientale e Geoingegneria, Consiglio Nazionale delle Ricerche, CNR-IGAG, RU Sapienza DICEA, 00184 Rome, Italy; alessandro.bosman@cnr.it
3 ISPRA Istituto Superiore per la Protezione e la Ricerca Ambientale Via Brancati, 00144 Rome, Italy; francesco.rende@isprambiente.it
4 Laboratorio Museo di Scienze della Terra Isola di Ustica, 90051 Palermo, Italy
5 Radboud Radio Lab, Department of Astrophysics/IMAPP, Radboud University-Nijmegen, 6500 GL Nijmegen, The Netherlands; a.vecchio@astro.ru.nl
6 Lesia Observatoire de Paris, Université PSL, CNRS, Sorbonne Université, Université de Paris, 92195 Meudon, France
7 School of Engineering, Università della Basilicata, 85100 Potenza, Italy; michele.greco@unibas.it
* Correspondence: daniele.trippanera@ingv.it

Abstract: The island of Ustica (Italy) is constantly exposed to the effects of sea-level rise, which is threatening its coastal zone. With the aim of assessing the sea levels that are anticipated by 2150 CE under the climatic projections shown in the AR6 report from the IPCC, a detailed evaluation of potential coastal flooding under different climatic scenarios and the ongoing land subsidence has been carried out for three coastal zones. Scenarios are based on the determination of the current coastline position, a high-resolution digital terrain and marine model, and the SSP1-2.6, SSP3-7.0, and SSP5-8.5 climatic projections. Relative sea-level rise projections allowed the mapping of the potential inundated surfaces for 2030, 2050, 2100, and 2150. The results show rising sea levels for 2150, ranging from a minimum of 66 ± 40 cm (IPCC AR6 SSP2.6 scenario) to a maximum of 128 ± 52 cm (IPCC AR6 SSP8.5 scenario). In such conditions, considering the SSP8.5 scenario during storm surges with return times (RTs) of 1 and 100 years, the expected maximum wave run-up along the island may vary from 3 m (RT = 1) to 14 m (RT = 100), according to the coastal morphology. Our results show that adaptation and mitigation actions are required to protect the touristic and harbor installations of the island.

Keywords: Ustica Island; vertical land movements; sea level rise projections; land subsidence; flooding scenario

Citation: Anzidei, M.; Trippanera, D.; Bosman, A.; Martin, F.F.; Doumaz, F.; Vecchio, A.; Serpelloni, E.; Alberti, T.; Rende, S.F.; Greco, M. Relative Sea-Level Rise Projections and Flooding Scenarios for 2150 CE for the Island of Ustica (Southern Tyrrhenian Sea, Italy). *J. Mar. Sci. Eng.* **2023**, *11*, 2013. https://doi.org/10.3390/jmse11102013

Academic Editor: Rodger Tomlinson

Received: 4 September 2023
Revised: 6 October 2023
Accepted: 16 October 2023
Published: 19 October 2023

1. Introduction

The island of Ustica is located in the southern Tyrrhenian Sea (see inset in Figure 1a). With a maximum elevation of 245 m a.s.l. (above sea level), it represents the emerging top of a vast submerged volcanic complex [1] rising more than 2850 m from the seafloor. The volcanism of Ustica is linked to the activation of a system of deep left transtensional faults (Figure 1a). The latter originated from the deformation events that accompanied the counterclockwise rotation of the Italian peninsula and the opening of the Tyrrhenian basin, following the complex interaction between the African and Eurasian plates [1].

The structural features of the island are driven by normal faults with a prevalent ENE–WSW and NE–SW trend, which reflect the regional tectonics [2].

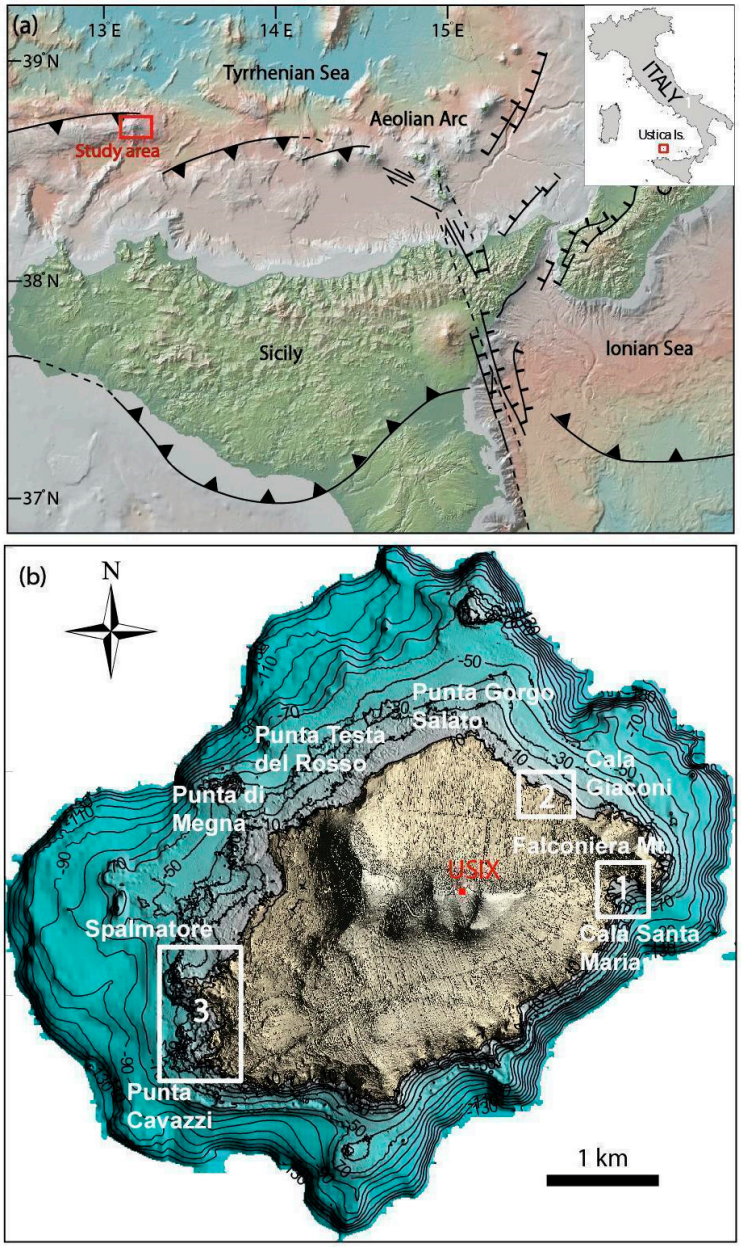

Figure 1. (**a**) Regional tectonic setting of the Eolian Arc and Ustica Island (red square); (**b**) offshore and onshore DEM of Ustica Island obtained by merging bathymetric and topographic LiDAR. The white rectangles indicate the areas surveyed by drone: 1—Ustica Harbor, 2—Ustica Northern Pier, and 3—Ustica Lighthouse (Punta Spalmatore). The inset shows the Ustica Island location (red square) with respect to Italy.

The volcanic activity ended around 130 ka BP, with the explosive hydromagmatic eruption of Monte Falconiera (157 m a.s.l.) and the formation of a tuff cone, the northern sector of which collapsed into the sea [1,3,4] (Figure 1b).

The subaerial sector of the volcanic edifice shows a predominant SW–NE orientation of about 4.5 km (major axis) and 2.7 km (minor axis) long (Figure 1b), which is affected by widespread erosional processes. The submerged sectors show similar orientation trends (with at least 130 m water depth). The current geomorphological structures of the emerged and submerged portions (up to −130 m water depth) represent the result of the complex interaction between glacio-eustatic sea-level fluctuations, erosion, and volcanic activity (light blue area in Figure 1b).

The topography shows more overlapping cycles of marine transgressions, resulting from the combination of vertical movements of the volcano edifice (due to the contribution of possible events of uplift and subsidence) and sea-level changes that occurred in the Middle-Upper Pleistocene, between 350 and 80 ka BP. The glacio-eustatic movements formed five main marine terraces that can be found at Piano dei Cardoni, Oliastrello, Tramontana, Arso, and Spalmatore. These terraces are presently found at variable heights of between 5 m and 120 m a.s.l. [5].

The island is separated into a northern and southern sector characterized by central reliefs with steep slopes [2,5].

From the coastline to −130 m in depth, the submarine flank of the volcanic edifice of Ustica is cut by an insular shelf (Figure 1b). It is characterized by gentle slopes (2–15°, but typically of less than 3°), which interrupt the morphological continuity between the steeper (>25°) subaerial and submarine flanks of the volcanic edifice (Figure 1b). In shallow waters, the shelf exhibits variable morphological characteristics, such as the width and depth of the shelf edge around the island. The widest and deepest shelves are observed along the W (Punta Spalmatore), NW (Punta di Megna), and N–NE (from Punta Testa del Rosso to Punta del Gorgo Salato) sectors. Conversely, in the southernmost sector, the shelf is absent and has been eroded due to a network of submarine channels and instability processes that are typical of submerged volcanic systems [6,7]. The erosional surface of the shelf in the northern sector is partially covered by sediments (mostly volcanic and bioclastic deposits), organized into submarine depositional terraces [5].

For the island of Ustica, the sea wave and tide data are available from the Palermo wave buoy (Figure S2 in the Supplementary Materials). The strongest waves that strike this sector come from a northwesterly direction, as the prevailing winds are from the northwest or west (Figure S1). The western and northern flanks of Ustica are affected by storms, with a typical fetch of 250–300 nautical miles and waves of up to 6 m (Figure S1; Tables S1 and S2). Southeasterly winds also affect the southeastern and eastern sides of the island, especially during autumn and winter, while the southern sector is sheltered by the nearby Sicily.

Based on their geomorphological features, the 20.5 km coastline of Ustica can be classified into four different coastal sectors (Figure 1b):

- The southern sector, positioned between Cala S. Maria and Punta Cavazzi. It is characterized by high (~80 m a.s.l.) and jagged cliffs that descend into the sea, with steep slopes characterized by basaltic rocks, hyaloclastite, and lava flows [6].
- The western sector, which lies along the coasts of Spalmatore. It is characterized by the lowest and most indented coast of the island and is formed from a succession of subaerial and submarine volcanic layers [6].
- The northern sector, which exhibits high cliffs of up to 40 m and faults. A stretch of cliff between 10 and 40 m high starts from Punta di Megna and continues up to Punta Gorgo Salato, resulting from a NE–SW-oriented fault. Another stretch of cliff, about 20 m high, starts from Punta del Gorgo Salato and continues up to Cala Giaconi. It arises from a fault aligned in the NW–SE direction [6,7].
- The eastern sector is characterized by the promontory of the Falconiera, which is the relict of a tuff cone that was active about 130 ka BP. On its northern side, there is the bottom of a semi-collapsed crater that fell into the sea, with its neck still evident [4,6].

To assess the potential impacts of global sea-level rise triggered by ongoing global warming [8,9], we have conducted a thorough evaluation of the expected coastal flooding up to the year 2150 for the different sea-level rise projections released by the IPCC www.ipcc.ch (accessed on 20 September 2023) in the AR6 Report. To this end, we included the current rate of local land subsidence (VLM), estimated via GNSS data collected by the geodetic INGV network. The assessment included high- and very high-resolution digital terrain and marine models extracted from LiDAR data and new photogrammetry surveys via UAV. Through these efforts, we were able to develop detailed multitemporal maps for 2030, 2050, 2100, and 2150 of the three most exposed coastal zones of the island, to model

the expected potential inundation scenarios, as well as in storm surge conditions, for return times of 1 and 100 years.

2. Materials and Methods

Our multidisciplinary study was planned in three main phases:

(1) Image collection by UAV surveys to obtain ultra-high-resolution DSMs and orthomosaic images of the three selected coastal zones. The latter were selected based on the presence of human facilities and on the different coastal morphology (an especially steep coastline made by lavas without beaches vs. a smoother coastline with wide beaches). These data were then calibrated and integrated with topographic LiDAR (see Section 2.1);
(2) Geodetic analysis for the estimation of the current rates of vertical land movement (VLM) from the GNSS station USIX, located in the inner island (Figure 1b);
(3) Incorporating geodetic and topographic data with the regional IPCC-AR6 projections (RCP-SSP2.6 and RCP-SSP8.5 climatic scenarios) to calculate the upper bounds of the expected sea levels for 2050, 2100, and 2150 CE.

The results of these three steps are used to map the current and the projected coastline positions to estimate the multitemporal expected inland extent of the marine flooding and shoreline positions.

An additional step concerns the analysis of storm surge scenarios (SS) in both actual and sea-level rise conditions, considering a storm surge intensity for return times of 1 and 100 years. In order to estimate the maximum wave level (MWL) seen in SS conditions around the island, we used the topographic and bathymetric data (see Section 2.1).

2.1. Topographic and Bathymetric Data

To generate the DTMM (digital terrain and marine model) of the entire island and its submerged portions (down to −130 m), different datasets with different resolutions were used. Airborne topographic LiDAR data with 2 m of ground resolution were made available by the Italian Ministry of the Environment. The density of the ground point cloud ranged from approximately 0.5 to 0.7 samples per square meter, collected in the form of ellipsoidal height (WGS84) and then converted to orthometric height using the Italgeo 2005 geoid model [10].

The bathymetric LiDAR survey, with a ground resolution of 2 m, was collected via LiDAR scanning on an aerial platform and performed by the Italian Ministry of the Environment. The survey covered the coastal strip facing the marine protected areas in the years from 2007 to 2013. A Fugro laser airborne depth sounder (LADS) MKII bathymetric LiDAR system was used to collect the data covering the shallow-water island. The point cloud density of the bathymetric data varied from approximately 0.1 to 0.2 samples per square meter. This allowed the generation of a 2.5 m DEM with a maximum water depth of approximately 63 m. The Italgeo 2005 model was also used to transform the bathymetric LiDAR data type from ellipsoidal height to orthometric elevation.

2.2. Aerial Photogrammetry and Digital Elevation Model Production

In our study, we applied state-of-the-art technology and techniques to aerial photogrammetry to produce very high-resolution digital surface models (DSMs) for three selected areas on Ustica Island. The aerial surveys were conducted in September 2019, using DJI Mavic 2 Pro (1″ CMOS lens and 20 M effective pixels). A total of 959 aerial digital photos were captured, with 70% of longitudinal and 70% of lateral overlap between subsequent images. This approach resulted in a ground sampling distance (GSD) of between 2 and 2.5 cm/px, covering a total area of 0.456 km^2 (see Table 1 for details). For enhanced accuracy, we placed a set of ground control points (GCPs) in each investigated area (Table 1). GCPs were measured using a multi-constellation and multi-frequency GNSS receiver in real-time kinematic mode. The GCP positions were estimated, with a planimetric accuracy ranging from 2 to 5 cm. To reconstruct the 3D point clouds and the

derived products, we used the structure from motion (SFM) technique [11,12]. We used the following homogeneous processing steps for each survey:

(1) To extract the orthometric elevation (that is, the elevation above sea level) for the determination of mean sea level, we corrected both the point cloud and the GNSS/RTK coordinates of the GCPs by using the Italgeo2005 model (from the Instituto Geografico Militare elevation grid).
(2) To mitigate the 3D model distortion inherent to the photogrammetric process, we used topographic LiDAR data as a reference frame to further constrain the photogrammetric model. To achieve this, we created several virtual GCPs in the common areas between the LiDAR data and drone survey (e.g., parking lots, buildings, roads, pavements, squares, docks, etc.), obtaining a final mismatch between the drone and LiDAR datasets on the order of maximum 10 cm on the Z component (see N.GCPs (LiDAR GCPs) in Table 2).
(3) Finally, DEMs were extracted through an interpolation of the photogrammetric point cloud, resulting in a final DEM resolution of approximately 3 cm/px (Table 1). The last step was to create an orthomosaic of each area by merging the orthorectified images using SFM Agisoft Metashape 2.0 software.
(4) In order to extract the coastline position, we generated contour lines from the DEMs. However, in areas where sea waves and water refraction hindered precise automatic reconstruction, we manually drew and adjusted the coastline using the orthomosaic as a reference.

Table 1. Flight information, ground control point (GCP) error estimates, output resolution, and ellipsoid corrections for the three surveys carried out at Ustica Island.

Survey Data	Northern Pier	Lighthouse	Harbor
number of images	179	726	54
flight altitude	85	90	105
GSD (cm/pixel)	1.97	2.02	2.46
covered area (m^2)	61,000	327,000	68,000
land area (m^2)	42,017	181,582	28,457
flight duration (min)	10	45	5
N.GCP (survey)	6	11	9
N.GCP (LiDAR GCP)	24	40	10
RMSE Z (m) compared to LiDAR	0.12	0.11	0.06
DEM resolution (m)	0.3	0.3	0.3
dense cloud points	228,611,527	237,752,605	80,091,741
exported CS	WGS84/UTM Zone 33N (EPSG: 32633)		
ellipsoid	ITALGEO 05		
survey data	21 September 2019	21 September 2019	22 September 2019

Table 2. Percentage of estimated flooded land surface in 2150 for the RSLR and SS scenarios, compared to the current land surface derived via aerial photogrammetry in 2019.

Coastal Area	RSLR Scenario for 2150 SSP5-8.5	RSLR Scenario for 2150 SSP5-8.5	SS Scenario for 2150 SSP5-8.5
Northern Pier	5.4%	18.4%	19.2%
Lighthouse	10.3%	50.6%	55.9%
Harbor	13.3%	50.1%	56.2%

Overall, this workflow ensured the accuracy and reliability of our results in mapping the coastline position and, subsequently, the extension of the potential coastal inundation due to sea-level rise.

2.3. Geodetic Data

Geodetic analysis includes tidal correction for the zero-elevation position and the high-water level (HWL), along with GNSS data for the estimation of the current VLM.

To estimate the current rate of VLM, we used the GNSS station USIX. This station belongs to the RING network managed by INGV and is located at the center of Ustica Island (Figure 1b). The crustal velocity for this station has been obtained, following the approach described in [13], which includes GNSS phase data reduction using GAMIT software v.10.71 [14].

According to our analysis, USIX shows a weak negative vertical geodetic velocity with an available position time-series in the time interval from 2005 to 2023, ensuring accurate vertical velocity and error estimates [13] that are consistent with the results from synthetic time-series calculations [15] and the lower bounds from real time-series calculations [13]. The current velocity of USIX corresponds to a land subsidence at -0.71 ± 0.35 mm/yr (Figure S3).

2.4. Storm Surge Analysis

The storm-surge scenario was derived by applying the consolidated approach used in maritime analysis. This takes into account the main components of wave climate assessment and wave transformation up to wave breaking to estimate wave conditions during the wave travel process. It finally ends with an assessment of the wave setup and run-up onto the coast for each transect.

Maritime wave climate assessment and storm surge data for the study areas have been evaluated using the forecast/hindcast system for the Mediterranean Sea, which was developed by the Department of Environmental, Chemistry, and Civil Engineering of the University of Genoa [16,17]. Wave climate assessment originates from a re-analysis of atmospheric and wave conditions, producing a hindcast database spanning from January 1979 until the end of December 2016, created over the domain employed for the atmospheric and wave-condition simulations.

The system is mainly based on the WAVEWATCH III (WWIII) model used in the Mediterranean. This model enables climate wave analysis, referring to several case studies related to heavy storms that were observed in this basin in the last twenty-five years. Wherever data were available, the simulation results have been validated using buoy data provided by different official sources.

Wind forcing has been simulated using the WRF (weather and research forecasting) model for all the case studies, while the wave simulations were carried out using the WWIII model. The simulated and observed data were compared via statistical error measures like normalized bias (NBI), the normalized root mean square error (NMRSE), also known as the scatter index, and the correlation coefficient (CORR). Since the model performances are not uniform in space and time, all the statistical error measures have been evaluated, taking into account the different groups of buoys chosen, depending on their geographical location in the Mediterranean basin or on the relevant sea conditions (either stormy or not stormy).

For the investigated site, the significant wave height polar histogram and the 2D histogram for the significant wave height, Hs, and peak period, Tp, were evaluated to derive the local wave climate scenarios, as well as an extreme value analysis (EVA) for the Hs. The extreme value analysis for all the available data has been carried out following the peak over threshold (POT) system, taking into account all peak storm event values exceeding the 98th percentile and imposing a minimum inter-arrival time between two storms of 12 h.

By the use of wave climate data referring to both ordinary and extreme storm wave conditions, in terms of the return period (RT), where RT = 1 year and RT = 100 years, wave setup and wave run-up were estimated. In the analysis, the wind setup was neglected. We used the topo-bathymetric information collected for each of the transects that were considered. For details on the analysis, see Table S2 in the Supplementary Materials.

2.5. Relative Sea-Level Rise Projections and Flooding Scenarios for 2050 and 2100 CE

To estimate future sea levels, we incorporated the contribution of VLM in the regional AR6 sea-level projections for the interval 2020–2150. The data are available from JPL at the Physical Oceanography Distributed Active Archive Center (PO-DAAC) https://podaac.jpl.nasa.gov/ (accessed on 20 September 2023).

These projections are obtained by summing up the contributions of several geophysical sources, such as the Antarctic Ice Sheet (AIS), the Greenland Ice Sheet (GIS), glaciers, land water storage, ocean dynamics (including thermal expansion), and VLM [8,9].

The data were provided for the shared socio-economic pathways (SSP1-1.9, SSP1-2.6, SSP2-4.5, SSP3-7.0, SSP5-8.5) and the global warming level (Tlim = 1.5 °C, 2 °C, 3 °C, 4 °C and 5 °C) scenarios considered in the AR6. In this study, we then revisited the AR6 sea-level projections by including the trend of the current VLM estimated from USIX GNSS stations, as described in Section 3. We assumed that the VLM rate would continue linearly up until 2150 with the same rate as today. However, we are aware that this assumption could diverge from the current VLM trend in the case of unpredictable volcanic or tectonic activity. Since the latter effects can even be long-term episodic events, a linear trend for the next few decades is the best approximation for incorporating the VLM signal into the relative sea-level projections presented in this study.

3. Results

The estimated relative sea level projections from 2020 to 2150 CE for three Socio-economic pathways (SSP1-2.6, SSP3-7.0, and SSP5-8.5) and global warming levels (Tlim 2 °C, 4 °C and 5 °C) for the investigated coastal tracts of Ustica Island are shown in Figure 2 and the corresponding values are reported in Table S1 (only regarding SSP scenarios).

The expected relative sea levels in the three SSP scenarios, corrected for a land subsidence of -0.71 ± 0.35 mm/yr, as recorded at the GNSS station USIX, correspond to a relative sea-level rise of 0.66 m, 1.13, and 1.28 m (with respect to 2020), respectively. This rise will trigger a continuous retreat of the coastline position (F see Sections 4.1–4.3). The upper limit of the expected RSLR for 2150 in the SSP5-8.5 scenario implies significant land flooding for the three study areas (see Table S1 for details).

Concerning the storm surges in RSLR conditions, our analysis shows that water levels (WL) along the northwest, north, and northeast coasts can reach elevations of 9.2 and 13.1 m (See Section 4.4). Along the southeastern coast, they reach an elevation of up to 5.6 m while nearby, in Ustica Harbor, the WL can reach 10 m (See Section 4.4).

Our results detail previous regional [18] and local [19–26] scenarios regarding RSLR along the coasts of the Mediterranean. In Section 4, we further discuss the main features of the three investigated coastal tracts and the related expected multitemporal flooding scenarios.

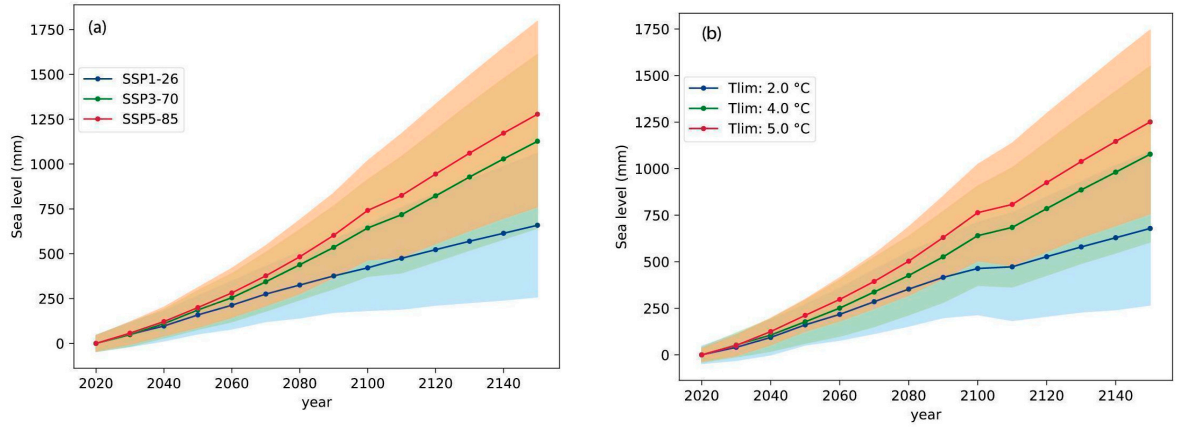

Figure 2. Sea-level rise projections for the coasts of Ustica Island from 2020 to 2150 CE. Projections are obtained by combining the SSP climatic projections reported in the Sixth Assessment Report (AR6) of the IPCC at regional scales, with the local VLM rate being derived from the GNSS analysis of the USIX station. The colored curves show the RSLR for SSP1-2.6, SSP3-7.and SSP5-8.5 scenarios (**a**) or are based on scenarios for temperature thresholds (Tlim) of 2.0 °C, 4.0 °C, and 5.0 °C (**b**). Colored areas show a 90% confidence interval.

4. Discussion

The rocky coasts of the island of Ustica are characterized by a stable dynamic system that facilitates an evaluation of the future changes in shoreline position occurring as a consequence of SLR. In particular, the lack of beaches, dune systems, and fine sediments prevent rapid changes of mass movement along the coast, as analyzed in other insular or continental areas of southern Italy [25,26]. Thus, the shorelines of Ustica in the next few decades are mainly elucidated with the combined effects of VLM and SLR. The maps and the cross-sections reported in Figures 3–9 show the initial detailed flooding scenarios due to RSLR in the investigated areas for 2030–2050–2100–2150 for the three different expected socio-economic pathways being considered. Our scenarios include the contribution of vertical land movements (due to global isostatic adjustment and vertical tectonics), which accelerate the submerging process of the investigated coastal tracts and allow us to estimate the extension of the expected marine submersion up until 2150, with the related potential impacts on coastal morphology and infrastructures.

Recent studies have identified that the risks associated with SLR in the Mediterranean are still poorly understood by the population [27]. Local-scale scientific data and visualization tools, such as digital maps, can be comprehended by citizens and stakeholders. Therefore, the maps of flooding hazards realized in this study and discussed in the following section can contribute to raising the awareness of local stakeholders and decision-makers to implement appropriate mitigation and adaptation policies for SLR.

4.1. Main Harbor

The area facing Ustica Harbor is a semi-enclosed inlet consisting of an open amphitheater to the southeast with relatively high slopes from 15° to 27°. The coastal area of the harbor consists of a pocket beach confined between the ship dock and the breakwater, with maximum elevations of up to about 2 m above sea level. The subaerial pocket beach is 85 m wide, with slopes of about 8° that drop sharply to about 2.5° for the submerged beach. The harbor area of the island is located at elevations of between about 0.6 and 3 m and hosts many receptive port facilities, such as roads, pavements, gas stations, and other facilities for mooring, commercial shipping, and nautical tourism.

Figure 3 shows the expected flooded area for the worst scenario, SSP5-8.5, for 2030 (yellow), 2050 (orange), 2100 (red), and 2150 (dark red). The dock and the beach will be severely flooded by 2100, while by 2150, about 13% of the whole harbor area will likely be submerged (Table 2). The cross-sections in Figure 3b show that in the absence of any

reinforcement works and the raising of the docks by 2150, the expected level of submersion could cause unusability of the port infrastructures and the retreat of about 50% of the beach. The external part of the breakwater will be partially submerged and will then be more exposed to storm surges and less able to protect the port basin (Figure 3a). A similar impact is expected by 2150 for an SSP3-7.0 scenario (Figures S5 and S6). Conversely, in the case of the most optimistic scenario, SSP1-2.6, the dock is safe and only almost $^{1}/_{3}$ of the beach will retreat (Figures S4 and S6).

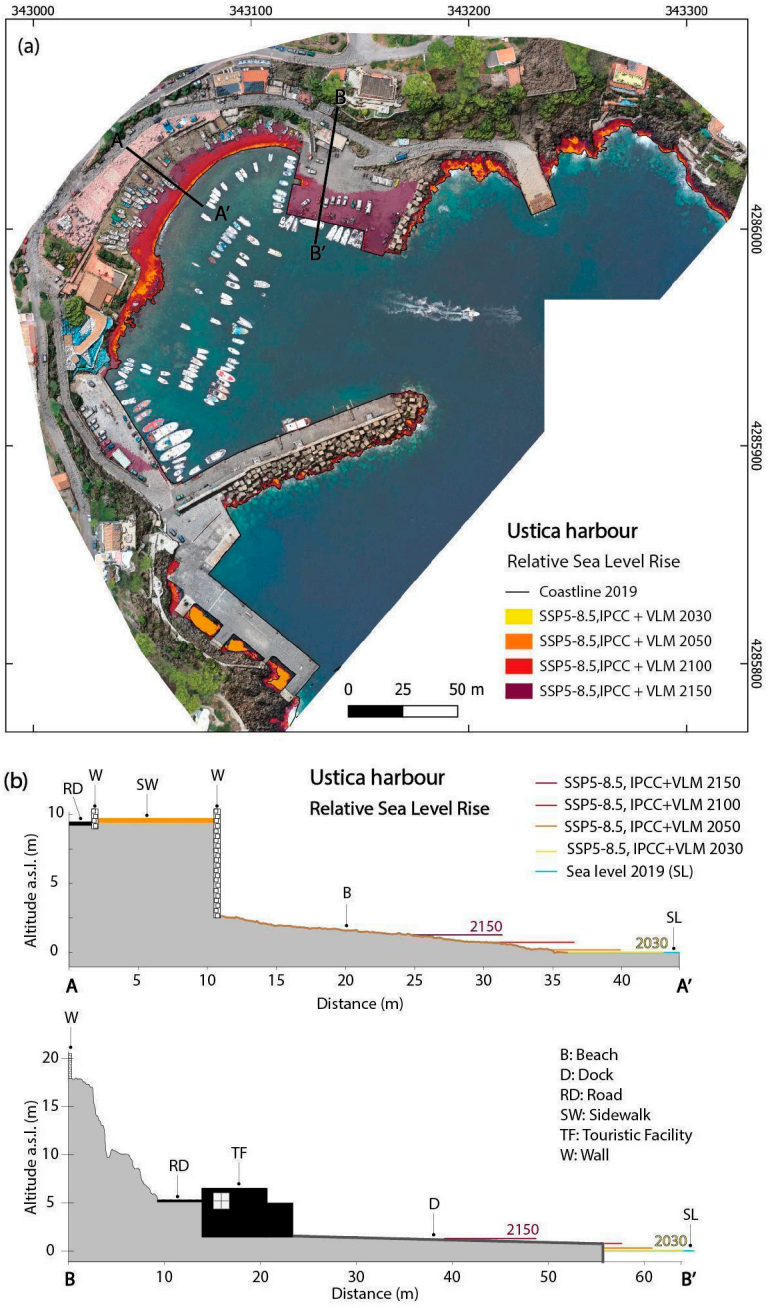

Figure 3. (**a**) Potential submersion areas for Ustica Harbor, based on the current rates of VLM and the SSP5-8.5 climatic scenario up until 2150 (see Table S1 and Figure 10a for flooded surfaces); (**b**) cross-sections of the expected RSLR for different SSP climatic projections up until 2150 across the beach (AA′) and the dock (BB′), as shown in panel (**a**).

4.2. Northern Pier

The coastal strip of this sector shows a high, rocky coastline consisting of steep cliffs up to 30 m above sea level, with slopes ranging from 25° to 80°. The seafloor at the foot of the cliffs is fairly flat, with the presence of a few rocky blocks in shallow water and a slope down to the sea with gradients ranging from 4° to 6°. Here, the most exposed infrastructure is the pier. Figure 4 shows the expected flooded area for the SSP5-8.5 scenario from 2030 to 2150. Due to the steep slope of the coast, even in the worst-case scenario, SSP5-8.5, the coastal tract exposed to submersion remains limited to about 5% with respect to the current surface (Table 2). Given the height of the pier above sea level, its surface will not remain exposed to submersion even in the worst-case scenario, SSP5-8.5 (Figure 4). For the other scenarios of SSP1-2.6 (Figure S7) and SSP3-7.0 (Figure S8), the expected impact is less severe.

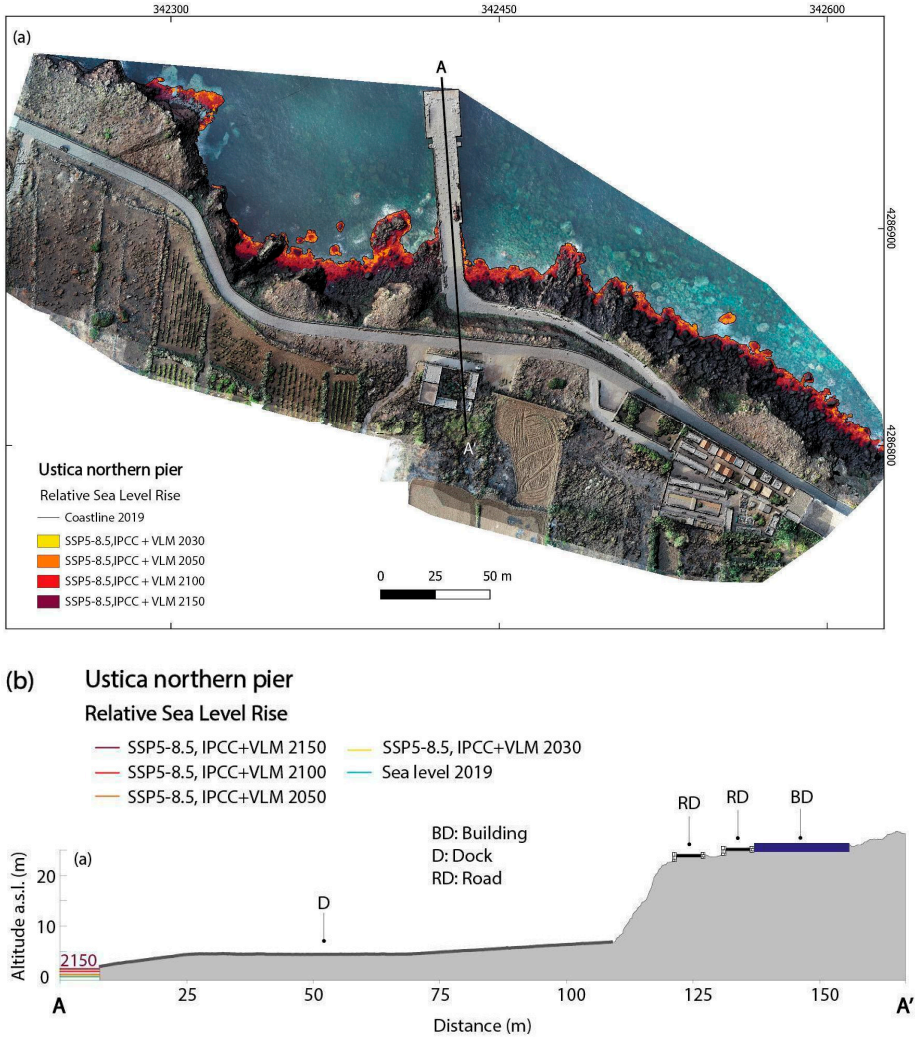

Figure 4. (**a**) Potential submersion areas for the northern pier, based on the current rates of VLM and the SSP5-8.5 climatic scenario up until 2150 (see Table S1 and Figure 10c for flooded surfaces); (**b**) cross-section of the expected RSLR for different SSP climatic projections up until 2150 across the pier (AA′), as shown in panel (**a**).

4.3. Punta Spalmatore Lighthouse

The coastal tract of Punta Spalmatore, where a lighthouse is located (from now on, known as the lighthouse), has lower elevations and slopes than the other two study areas, with coastal elevations ranging from a few meters up to 15 m above sea level. In contrast, here, the coastline is indented and is characterized by low elevated cliffs consisting of

rocky outcrops that form interdigitations and small inlets. In this area, there are two pocket beaches located in small semi-enclosed inlets, one of which includes a concrete platform for a touristic installation. The topography of the two pocket beaches shows high slopes varying from 5° to 7°. The coastal area of the lighthouse has a few housing structures at elevations ranging from 10 m to about 15 m, with small accommodation facilities for bathing activities located between 1 m and 4 m above sea level.

Figure 5a shows the expected flooded area for the SSP5-8.5 scenario between 2030 and 2150. The two pocket beaches (for location, see cross-sections A-A' and B-B' in Figure 5b) will already be partially flooded by 2100, while about 10.3% of the surveyed coast will be submerged by 2150 (Table 2). The cross-sections in Figure 5b show that by 2150, the expected RSLR will likely cause the submersion of both pocket beaches and the unusability of the touristic infrastructures as a consequence of marine flooding.

Given the height of the lighthouse building above sea level, this structure will not be exposed to submersion, even in the worst-case scenario of SSP5-8.5 (Figure 5b). The pocket beaches will be affected by the sea-level rise, even in the more optimistic scenarios of SSP1-2.6 (Figures S9 and S10) and SSP3-7.0 (Figures S11 and S12). In particular, the southern beach will be almost completely submerged in the SSP3-7.0 scenario by 2150.

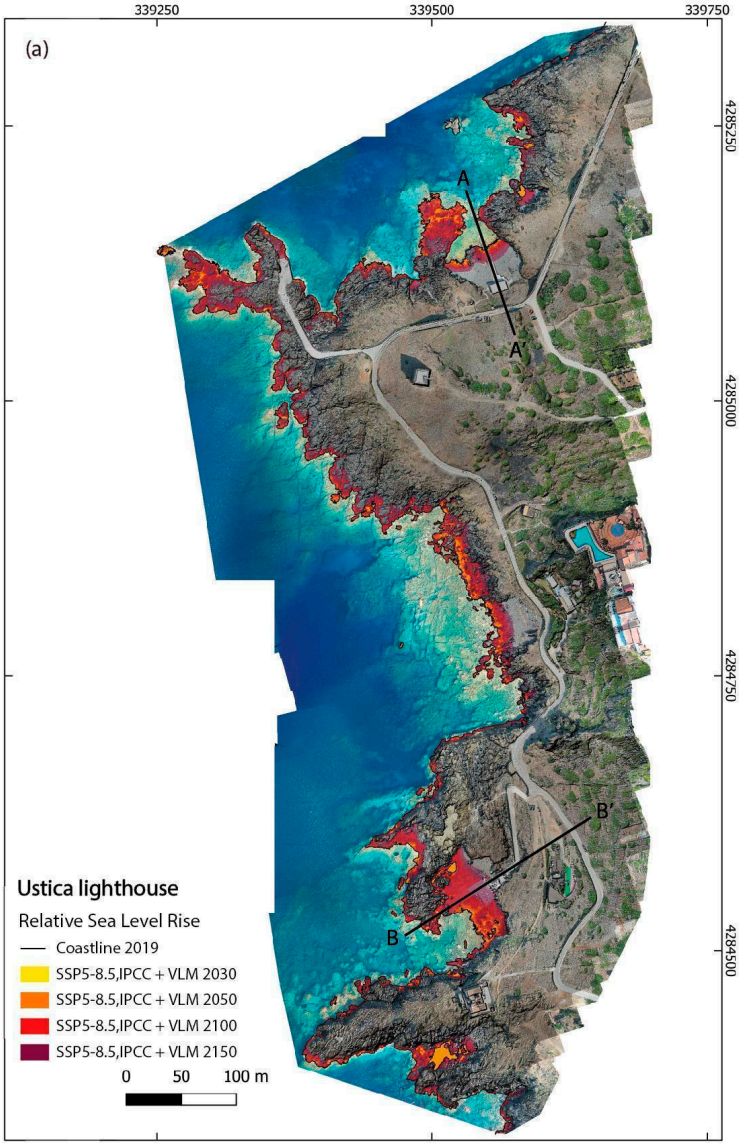

Figure 5. *Cont.*

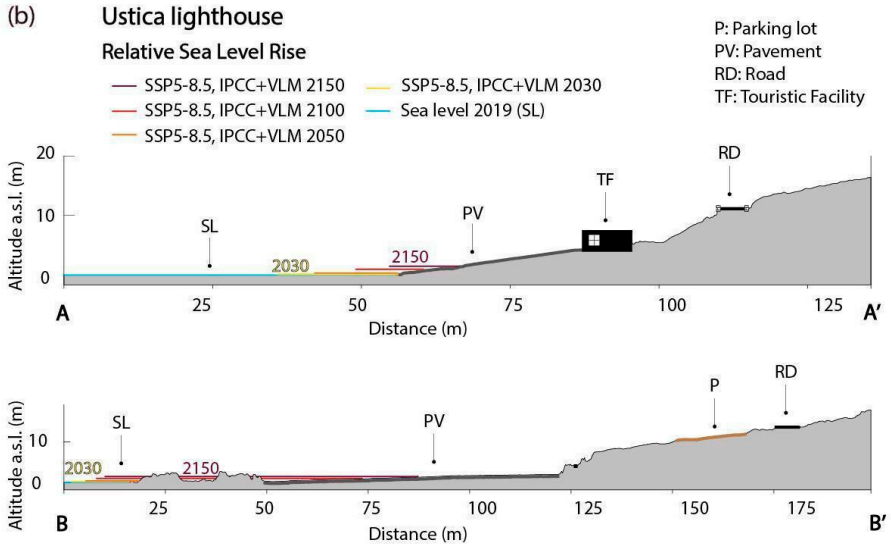

Figure 5. (**a**) Potential submersion areas for Ustica Lighthouse, based on the current rates of VLM and the SSP5-8.5 climatic scenario up until 2150 (see Table S1 and Figure 10b for flooded surfaces); (**b**) cross-sections of the expected RSLR up until 2150 for different SSP5-8.5 climatic projections across the northern (AA') and southern (BB') pocket beaches, as shown in panel (**a**).

4.4. Storm Surge Scenarios

Concerning the flooding effects of storm surges, we first considered their impact on the whole island by using the available topography drawn from the LiDAR and bathymetric data. Then we analyzed in detail the storm impact in the three areas where the drone datasets have been acquired.

For the whole island, we calculated the maximum run-up values for storm surge events with return times of 1 and 100 years (Figure 6 and Table S2) along 18 cross-sections around the island (numbered dots in Figure 6). These values have been estimated considering both the year 2019 (Figure 6a and cross-sections in Figure 6c–f) and the year 2150 for an SSP5-8.5 scenario (Figure 6b and cross-sections in Figure 6c–f) as a sea-level reference in ordinary conditions. In particular, for events where RT = 100, the water levels (WL) during storm waves approaching the coast from the northwest, north, and northeast can reach elevations of 9.2 and 13.1 m, while for the southeastern sectors, they reach an elevation up to 5.6 m, with the exception of the coast of Falconiera, near to Ustica Harbor, where the WL can reach 10 m. It is worth noting that the northwest, northern, and northeastern sectors of the coasts are exposed to the longest fetches. Despite the lower sloping seafloor morphology with respect to the southern coastal sector, the amplitude of maximum WL is higher (see also the Supplementary Materials for Table S2).

The impact of a storm surge can be studied in detail in the three areas surveyed with the drone (yielding higher terrain model accuracy compared to the topographic radar). While the estimates of WL due to an overall sea-level rise in static conditions are the same for the three areas, the maximum WL due to a storm surge may be different, due to the different coastal morphology and exposure to the wind (Table S1).

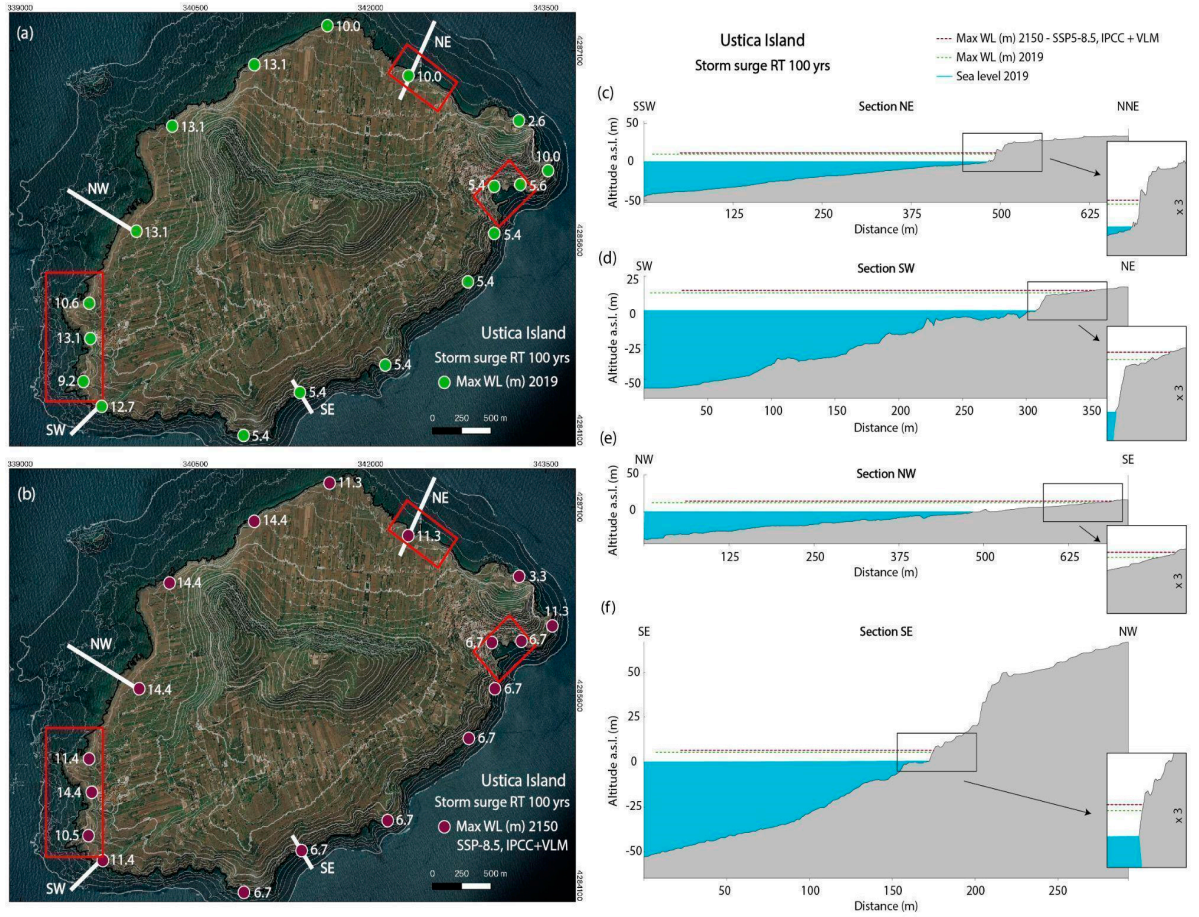

Figure 6. Left: The potential maximum water levels (max WL, shown in white numbers) for 18 coastal zones (red dots) on Ustica Island for a storm surge with a return time (RT) of 100 years, based on (**a**) the 2019 sea level and (**b**) in RSLR conditions for the SSP5-8.5 climatic scenario, for the year 2150. See the main text for further details. **Right**: The potential maximum water level (max WL) along four representative cross-sections for a storm surge with a return time (RT) of 100 years, based on the 2019 sea level (green dashed lines) and RSLR conditions for the SSP5-8.5 climatic scenario for the year 2150 (red dashed lines). (**c**–**f**) Cross-sections along the NE, SW, NW, and SE lines (in Figure 6a,b). See Table S2 for further details.

The expected sea-level rise in ordinary conditions for the worst predicting scenario (SSP5-8.5) by 2150 is about 1.3 m. In the harbor area, the WL during a storm surge may currently reach a maximum of 5.4 m (almost four times higher, if compared to the RSLR) and up to 5.6 m by 2150 (Table S1, Figure 7). As a consequence, assuming a sea-level rise scenario in static conditions, 13% of the land will be flooded by 2150, and up to 50% (using the 2019 reference epoch) and 56% (using the 2150 reference epoch) of land will be affected by seawater (Table 2 and Figure 7) in the case of a violent storm surge (RT 100). This implies the submersion of the road to the harbor, the dock, and the touristic facilities closer to the sea, along with the beach and the breakwater (Figure 7). When assuming a storm surge with an RT of 1 year, the WL is almost the same for this area (Table S2).

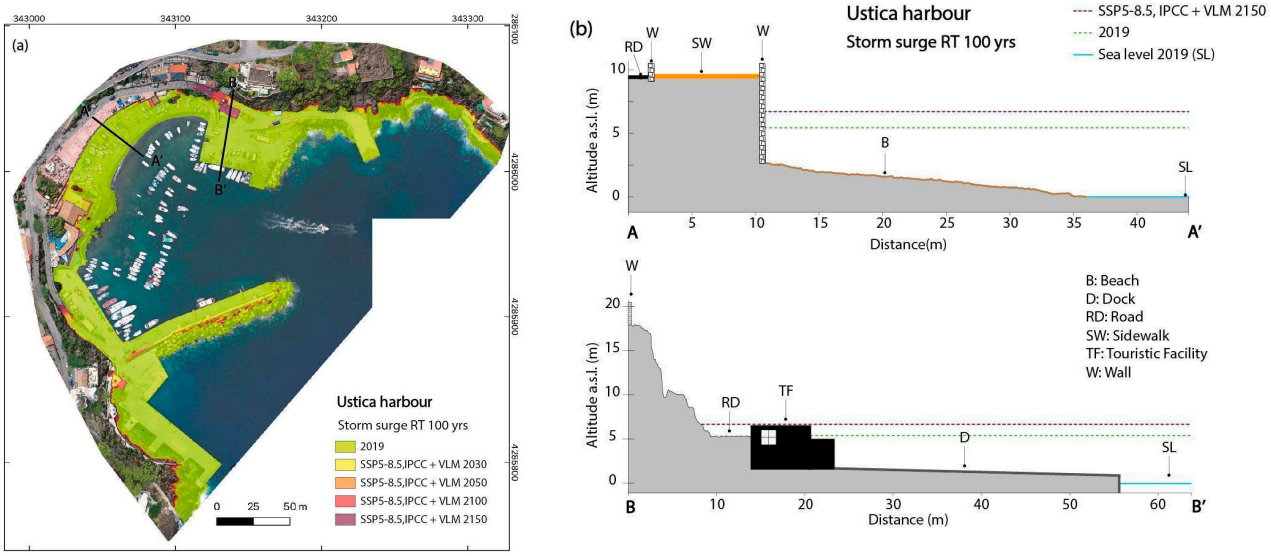

Figure 7. (**a**) The potential submersion areas for Ustica Harbor in storm surge conditions for a return time (RT) of 100 years, based on the 2019 sea level and the RSLR conditions in 2150 for the SSP5-8.5 climatic scenario (see Table S1 and Figure 10a for flooded surfaces); (**b**) potential maximum water level (max WL) for a storm surge with a return time (RT) of 100 years, based on the 2019 sea level (green dashed lines) and RSLR conditions for the SSP5-8.5 climatic scenario for the year 2150 (red dashed lines) across the beach (AA') and the dock (BB') sections, as reported in Figure 7a.

For the northern pier, the WL calculated for a storm surge with RT = 1 is 6.5 m for the 2019 reference epoch and 7.7 m, assuming a sea-level rise by 2150 (SSP5-8.5) (Table S2). These values increase during a storm surge with RT = 100 (Tables S1 and S2). The WL may reach up to 10.0 m or 11.3 m for the 2019 and 2150 (SSP5-8.5 scenario) reference epochs, respectively (Table S1). This implies that the dock will be entirely covered by the water (Figure 8). Our data suggest that while only 5.4% of the land will be flooded by 2150 in static conditions, a storm surge occurrence (with RT = 100) may flood up to 18.4% (2019) and 19.2% (2150) of the land surface (Table 2).

In the Punta Spalmatore lighthouse area, the sea level in a storm surge with RT = 1 may reach up to 6.7 m (2019) and 8 m (2150; SSP5-8.5 scenario) (Table S2). Also in this area, the WL value, assuming a more severe storm surge (RT = 100), may increase to 10.2 m (2019) and 11.4 m (2150, SSP5-8.5 scenario) (Table S1) with flooding over 50.6% and 55.9% of the land by 2019 and the 2150 epochs (Figure 9). This percentage is much higher compared to that for the flooded surface by 2150, due to the overall RSLR (10.3%) (Figure 10). The touristic facilities, the pocket beach, and the pavements will be inundated by the water during a storm surge (Figure 9).

The smaller increase in the percentage of flooded land in the northern pier sector estimated for static RSLR and storm surge scenarios can be attributed to the steep topographic features of the coastal zone, which prevent storm surge waves from increasing their run-up during extreme events. Our predictions can be confirmed by the pictures from previous storm events in Ustica Island (Figure 11).

Figure 10 shows the time-dependent increasing extension of the expected flooded surface for the three analyzed climatic scenarios (SSP1-2.6; SSP3-7.0; SSP5-8.5) for the harbor, lighthouse, and northern pier areas for 2030, 2050, 2100, and 2150. This includes the effects of VLM. In the same figure, we also show a comparison between the potential flooded surfaces, based on the VLM + SLR projections for the SSP5-8.5 climatic scenario (black), versus a storm surge with a return time (RT) of 100 years (gray).

In general, assuming that the reference topography will not change significantly between 2019 and 2150, the maximum water level due to a storm surge with an RT of 100, using the year 2019 as the reference epoch, is almost similar to the water level obtained for

the year 2150 (considering an SSP5-8.5 scenario) (Table S2). Conversely, the impact of such a storm is much more dramatic than the sea-level rise itself.

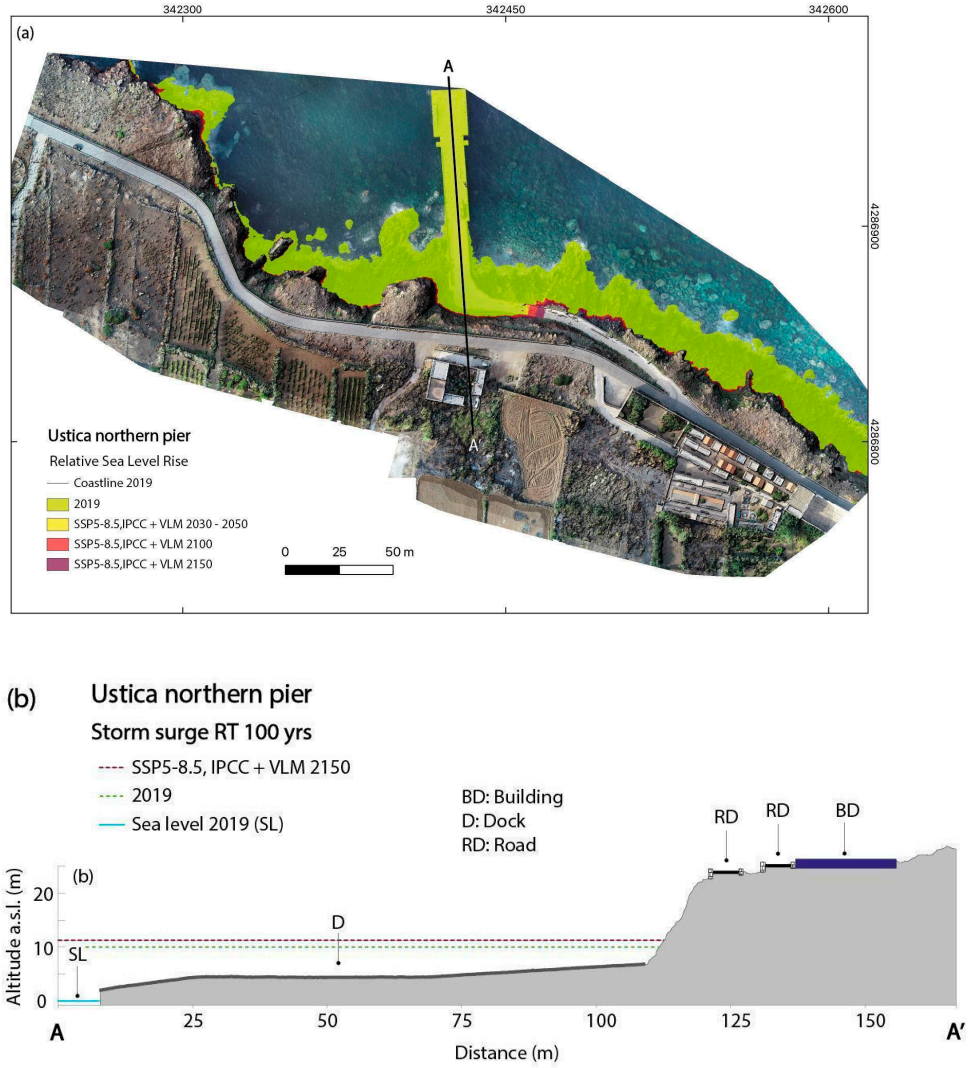

Figure 8. (**a**) The potential submersion areas of Ustica Northern Pier for a storm surge with a return time (RT) of 100 years, based on the 2019 sea level and RSLR conditions and an SSP5-8.5 climatic scenario in the year 2150 (see Table S1 and Figure 10 for flooded surfaces); (**b**) potential maximum water level (max WL) for a storm surge with a return time (RT) of 100 years, based on the 2019 sea level (green dashed lines) and RSLR conditions for an SSP5-8.5 climatic scenario in the year 2150 (red dashed lines) across the northern pier (AA'); the sections are shown in Figure 8a.

For any of the considered RSLR scenarios, in sea-level rise conditions, the increasing wave energy along the coast is to be expected, leading to accelerated beach erosion and enhanced damage to harbor installations [28].

Finally, because flooded areas have been estimated with respect to the local mean sea level, during exceptionally high tides or extreme events, such as a tsunami, the sea may temporarily flood larger surface areas [29].

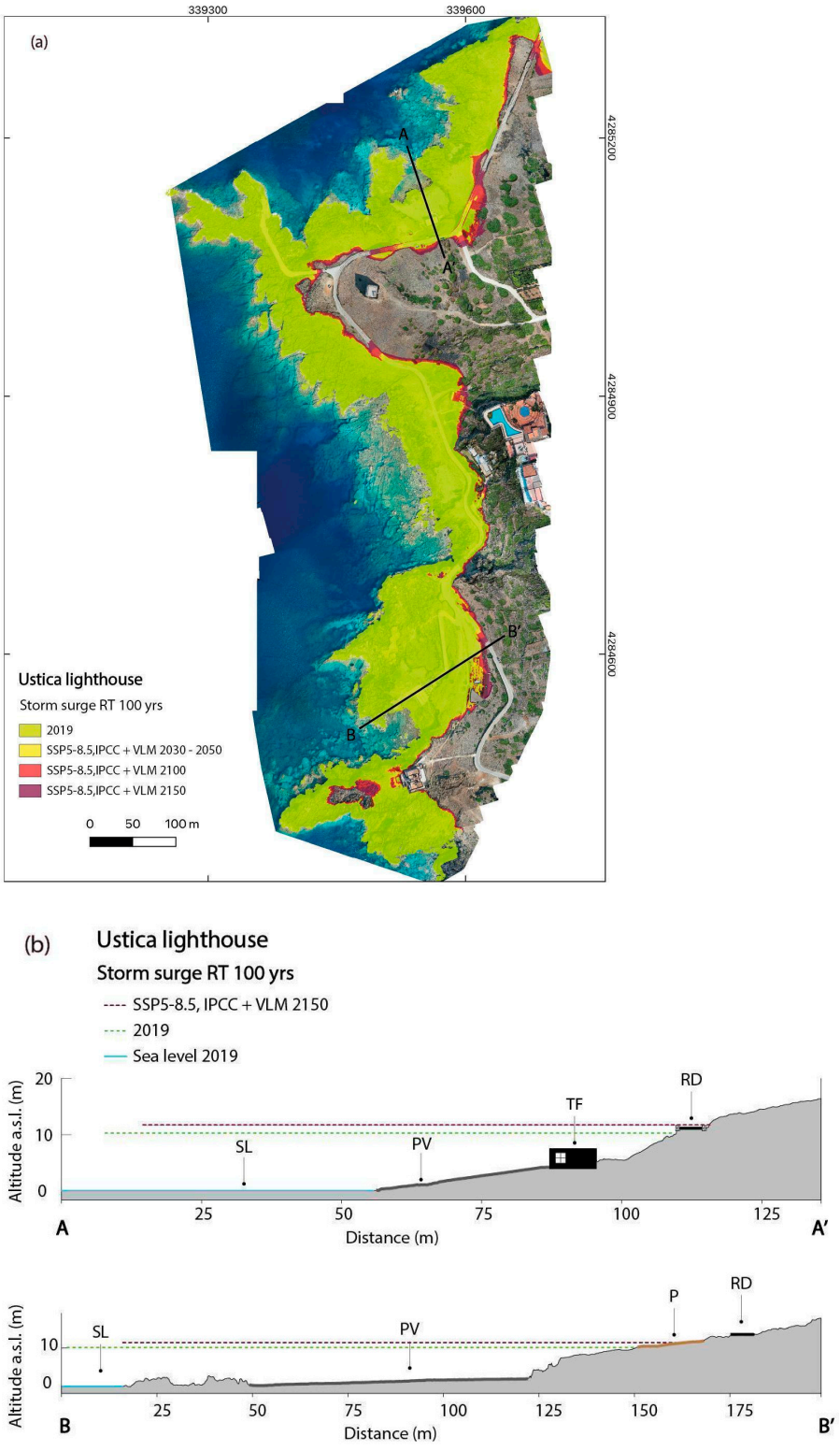

Figure 9. (**a**) The potential submersion areas at Ustica Lighthouse for a storm surge with a return time (RT) of 100 years, based on the 2019 sea level and RSLR conditions for an SSP5-8.5 climatic scenario in the year 2150 (see Table S1 and Figure 10b for flooded surfaces); (**b**) potential maximum water level (max WL) for a storm surge with a return time (RT) of 100 years, based on the 2019 sea level (green dashed lines) and RSLR conditions for an SSP5-8.5 climatic scenario in the year 2150 (red dashed lines) across the northern (AA′) and the southern (BB′) pocket beaches; the sections are shown in Figure 9a.

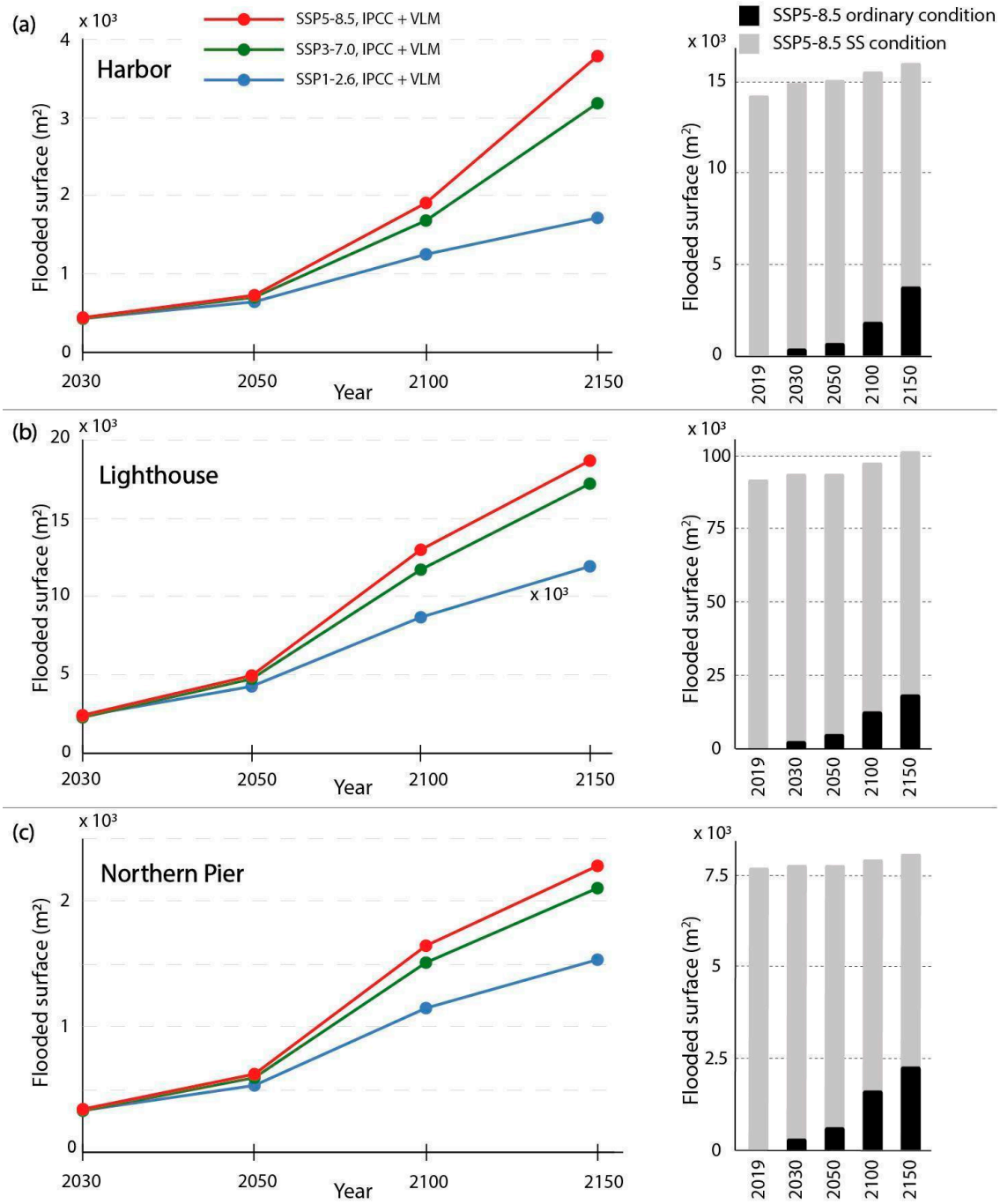

Figure 10. Left: Extension of the expected flooded surfaces for the (**a**) harbor, (**b**) lighthouse, and (**c**) northern pier, based on the RSLR projections for the SSP1-2.6 (blue), SSP3-7.0 (green) and SSP5-8.5 (red) climatic scenarios for 2030, 2050, 2100, and 2150 (see Table S1). **Right**: Comparison of the extension of potentially flooded surfaces for the (**a**) harbor, (**b**) lighthouse, and (**c**) northern pier areas for 2030, 2050, 2100, and 2150, based on the RSLR projections for an SSP5-8.5 climatic scenario (black) and a storm surge with a return time (RT) of 1800 years, based on the 2019 sea level and RSLR conditions for an SSP5-8.5 climatic scenario (gray) (see Table S1).

Figure 11. Photos of storm surge events along the coast of Ustica: (**a**,**b**) the harbor; (**c**) the lighthouse of Punta Spalmatore; (**d**) the northern pier. (**a**–**c**) Photo credits: Vincenzo Padovani; (**d**) Pietro Bertucci, Ustica sape.

5. Conclusions

Due to its morphological and geological features and the low rate of land subsidence, the island of Ustica is only partially affected by the expected RSLR levels. The lack of large sandy beaches and low-elevation coasts and the steep slope of the cliffs limit the island's exposure to flooding risk resulting from the RSLR in the coming decades.

The most exposed sector is the harbor area, where the RSLR and the increased effects of SS in RSLR conditions will significantly impact on port infrastructures and touristic and commercial installations, particularly starting from the year 2100.

In RSLR conditions, the coastal zone at the foot of the lighthouse area would be highly exposed to the submersion of the pocket beaches as well as the touristic infrastructures, with potential economic losses. The structure of the lighthouse, being placed at a safe altitude above the sea level, will only be slightly impacted during extreme SS events.

The north pier area is the least exposed to RSLR, due to the steep high cliffs that characterize this coastal tract. However, the present pier is already exposed to SS events, limiting its usability in case of extreme events in RSLR conditions before 2100.

The methodological approach presented in this study can be applied worldwide in coastal areas that are exposed to SLR due to the combination of global warming and vertical land movement. In this regard, land planners and decision-makers should take into account SLR projections and flooding scenarios similar to those reported in this study for cognizant coastal management, to ensure the preparedness of local populations and the protection of coastal infrastructures regarding expected changes.

Supplementary Materials: The following supporting information can be downloaded at: https://www.mdpi.com/article/10.3390/jmse11102013/s1, SM1, Figures S1–S12, Tables S1 and S2 [30–34].

Author Contributions: Conceptualization, M.A., D.T., A.B. and M.G.; methodology, M.A., A.B., M.G. and A.V.; software, M.G., A.V., D.T. and A.B.; formal analysis, A.V., M.G., D.T., E.S., T.A. and S.F.R.; investigation, M.A. and F.D.; resources, M.A.; data curation, D.T. and A.B.; writing—original draft preparation, M.A. and F.F.M.; writing—review and editing, M.A., D.T. and A.B.; visualization, F.D.; supervision, M.A., A.V. and A.B.; project administration, M.A.; funding acquisition, M.A. All authors have read and agreed to the published version of the manuscript.

Funding: This research was funded by Pianeta Dinamico Project MIUR 2020–2029 Working Earth –"Working Earth: geosciences and understanding of the earth dynamics and natural hazards" (CUP D53J19000170001). (Resp. Prof. Carlo Doglioni; Resp. Scientifico Dr. Guido Ventura) directed by INGV under the umbrella of the Italian Ministry of Research. This study benefited from the methodology developed in SAVEMEDCOASTS (agreement number ECHO/SUB/2016/742473/PREV16 www.savemedcoasts.eu, accessed on 20 September 2023) and SAVEMEDCOASTS2 (project number 874398 www.savemedcoasts2.eu, accessed on 20 September 2023) projects, both funded by the European Commission through the DG-ECHO.

Informed Consent Statement: Informed consent was obtained from all subjects involved in the study.

Data Availability Statement: Aerial photogrammetric data were collected by the authors. LiDAR data were provided by the Sicily Region. GNSS data were retrieved, processed, and archived by the INGV geodetic analysis data center. The analysis was performed using the GAMIT/GLOBK software v.10.71 at INGV-Bologna. Tidal data were obtained from www.mareografico.it (accessed on 20 September 2023).

Acknowledgments: We acknowledge the Municipality of Ustica for its kind collaboration during the aerial surveys.

Conflicts of Interest: The authors declare no conflict of interest.

References

1. de Vita, S.; Guzzetta, G.; Orsi, G. Deformational features of the Ustica volcanic area in the Southern Tyrrhenian Sea (Italy). *Terra Nova* **1995**, *7*, 623–629. [CrossRef]
2. Cinque, A.; Civetta, L.; Orsi, G.; Peccerillo, A. Geology and geochemistry of the island of Ustica (Southern Tyrrhenian Sea). *Rend. Soc. It. Min. Petr.* **1988**, *43*, 987–1002.
3. de Vita, S.; Laurenzi, M.; Orsi, G.; Voltaggio, M. Application of 40Ar/39Ar and 230Th dating methods to the chronostratigraphy of Quaternary basaltic volcanic areas: The Ustica island case history. *Quat. Int.* **1998**, *47/48*, 117–127. [CrossRef]
4. de Vita, S.; Martin, F.F. The palaeogeographic setting and the local environmental impact of the 130 ka Falconiera tuff-cone eruption (Ustica island, Italy). *Ann. Geophys.* **2017**, *60*, 2. [CrossRef]
5. Sulli, A.; Zizzo, E.; Spatola, D.; Morticelli, M.G.; Agate, M.; Iacono, C.L.; Gargano, F.; Pepe, F.; Ciaccio, G. Growth and geomorphic evolution of the Ustica volcanic complex at the Africa-Europe plate margin (Tyrrhenian Sea). *Geomorphology* **2021**, *374*, 107526. [CrossRef]
6. Furlani, S.; Antonioli, F.; Cavallaro, D.; Chirco, P.; Caldareri, F.; Martin, F.F.; Agate, M. Tidal notches, coastal landforms and relative sea-level changes during the Late Quaternary at Ustica Island (Tyrrhenian Sea, Italy). *Geomorphology* **2017**, *299*, 94–106. [CrossRef]
7. Furlani, S.; Foresta Martin, F. Headland or stack? Paleogeographic reconstruction of the coast at the Faraglioni Middle Bronze Age Village (Ustica island, Italy). *Ann. Geophys.* **2019**, *62*, 1. [CrossRef]
8. Fox-Kemper, B.; Hewitt, H.T.; Xiao, C.; Aðalgeirsdóttir, G.; Drijfhout, S.S.; Edwards, T.L.; Golledge, N.R.; Hemer, M.; Kopp, R.E.; Krinner, G.; et al. Ocean, cryosphere, and sea level change. In *Climate Change: The Physical Science Basis. Contribution of Working Group I to the Sixth Assessment Report of the Intergovernmental Panel on Climate Change*; Masson-Delmotte, V., Zhai, P., Pirani, A., Eds.; Cambridge University Press: Cambridge, UK, 2021.
9. Oppenheimer, M.; Glavovic, B.; Hinkel, J.; van de Wal, R.; Magnan, A.K.; Abd-Elgawad, A.; Cai, R.; Cifuentes-Jara, M.; DeConto, R.M.; Gosh, T.; et al. Chapter 4: Sea level rise and implications for low lying islands, coasts and communities. In *IPCC Special Report on the Ocean and Cryosphere in a Changing Climate*; Pörtner, H.O., Roberts, D.C., Masson-Delmotte, V., Eds.; Cambridge University Press: Cambridge, UK, 2021.
10. Barzaghi, R.; Borghi, A.; Carrion, D.; Sona, G. Refining the estimate of the Italian quasi-geoid. *Boll. Geod. E Sci. Affin.* **2017**, *66*, 145–159.
11. Ullman, S. The interpretation of structure from motion. *Proc. R. Soc. Lond. Ser.* **1979**, *203*, 405–426.
12. Colomina, I.; Molina, P. Unmanned aerial systems for photogrammetry and remote sensing: A review. *ISPRS J. Photogramm. Remote Sens.* **2014**, *92*, 79–97. [CrossRef]
13. Serpelloni, E.; Cavaliere, A.; Martelli, L.; Pintori, F.; Anderlini, L.; Borghi, A.; Randazzo, D.; Bruni, S.; Devoti, R.; Perfetti, P.; et al. Surface Velocities and Strain-Rates in the Euro-Mediterranean Region: From Massive GPS Data Processing. *Front. Earth Sci.* **2022**, *10*, 907897. [CrossRef]
14. Herring, T.A.; King, R.W.; McClusky, S.C. *GAMIT Reference Manual, Release 10.4*; Massachusetts Institute of Technology: Cambridge, MA, USA, 2010.
15. Masson, C.; Mazzotti, S.; Vernant, P.; Doerflinger, E. Extracting Small Deformation beyond Individual Station Precision from Dense Global Navigation Satellite System (GNSS) Networks in France and Western Europe. *Solid Earth.* **2019**, *10*, 1905–1920. [CrossRef]

16. Mentaschi, L.; Besio, G.; Cassola, F.; Mazzino, A. Developing and validating a forecast/hindcast system for the Mediterranean Sea. *J. Coast. Res.* **2013**, *65*, 1551–1556. [CrossRef]
17. Mentaschi, L.; Pérez, J.; Besio, G.; Mendez, F.J.; Menendez, M. Parameterization of unresolved obstacles in wave modelling: A source term approach. *Ocean. Model.* **2015**, *96*, 93–102. [CrossRef]
18. Lambeck, K.; Antonioli, F.; Anzidei, M.; Ferranti, L.; Leoni, G.; Scicchitano, G.; Silenzi, S. Sea level change along the Italian coast during the Holocene and projections for the future. *Quat. Int.* **2011**, *232*, 250–257. [CrossRef]
19. Anzidei, M.; Bosman, A.; Carluccio, R.; Casalbore, D.; D'Ajello Caracciolo, F.; Esposito, A.; Nicolosi, I.; Pietrantonio, G.; Vecchio, A.; Carmisciano, C.; et al. Flooding scenarios due to land subsidence and sea-level rise: A case study for Lipari Island (Italy). *Terra Nova* **2017**, *29*, 44–51. [CrossRef]
20. Anzidei, M.; Scicchitano, G.; Tarascio, S.; De Guidi, G.; Monaco, C.; Barreca, G.; Mazza, G.; Serpelloni, E.; Vecchio, A. Coastal retreat and marine flooding scenario for 2100: A case study along the coast of Maddalena Peninsula (southeastern Sicily). *Geogr. Fis. Dinam. Quat.* **2018**, *41*, 5–16.
21. Ravanelli, R.; Riguzzi, F.; Anzidei, M.; Vecchio, A.; Nigro, L.; Spagnoli, F.; Crespi, M. Sea level rise scenario for 2100 A.D. for the archaeological site of Motya. *Rend. Fis. Acc. Lincei* **2019**, *30*, 747–757. [CrossRef]
22. Anzidei, M.; Doumaz, F.; Vecchio, A.; Serpelloni, E.; Pizzimenti, L.; Civico, R.; Greco, M.; Martino, G.; Enei, F. Sea Level Rise Scenario for 2100 A.D. in the Heritage Site of Pyrgi (Santa Severa, Italy). *J. Mar. Sci. Eng.* **2020**, *8*, 64. [CrossRef]
23. Antonioli, F.; De Falco, G.; Lo Presti, V.; Moretti, L.; Scardino, G.; Anzidei, M.; Bonaldo, D.; Carniel, S.; Leoni, G.; Furlani, S.; et al. Relative Sea-Level Rise and Potential Submersion Risk for 2100 on 16 Coastal Plains of the Mediterranean Sea. *Water* **2020**, *12*, 2173. [CrossRef]
24. Anzidei, M.; Scicchitano, G.; Scardino, G.; Bignami, C.; Tolomei, C.; Vecchio, A.; Serpelloni, E.; De Santis, V.; Monaco, C.; Milella, M.; et al. Relative Sea-Level Rise Scenario for 2100 along the Coast of South Eastern Sicily (Italy) by InSAR Data, Satellite Images and High-Resolution Topography. *Remote Sens.* **2021**, *13*, 1108. [CrossRef]
25. Scardino, G.; Anzidei, M.; Petio, P.; Serpelloni, E.; De Santis, V.; Rizzo, A.; Liso, S.I.; Zingaro, M.; Capolongo, D.; Vecchio, A.; et al. The Impact of Future Sea-Level Rise on Low-Lying Subsiding Coasts: A Case Study of Tavoliere Delle Puglie (Southern Italy). *Remote Sens.* **2022**, *14*, 4936. [CrossRef]
26. Romagnoli, C.; Bosman, A.; Casalbore, D.; Anzidei, M.; Doumaz, F.; Bonaventura, F.; Meli, M.; Verdirame, C. Coastal Erosion and Flooding Threaten Low-Lying Coastal Tracts at Lipari (Aeolian Islands, Italy). *Remote Sens.* **2022**, *14*, 2960. [CrossRef]
27. Loizidou, X.I.; Orthodoxou, D.L.; Loizides, M.I.; Petsa, D.; Anzidei, M. Adapting to sea level rise: Participatory, solution-oriented policy tools in vulnerable Mediterranean areas. *Environ. Syst. Decis.* **2023**, 1–19. [CrossRef]
28. Masselink, G.; Hughes, M.G. *Introduction to Coastal Processes and Geomorphology*; McCann, S.B., Ed.; Edward Arnold: London, UK, 2003; Volume 354, p. 1980.
29. Chiocci, F.L.; Romagnoli, C.; Tommasi, P.; Bosman, A. The Stromboli 2002 tsunamigenic submarine slide: Characteristics and possible failure mechanisms. *J. Geophys. Res.* **2008**, *113*, B10102. [CrossRef]
30. Komar, P.D.; Gaughan, M.K. Airy wave theory and breaker height prediction. In *Proceedings of the 13th Coastal Engineering Conference*; Americcan Society of Civil Engineers: Reston, VA, USA, 1973; pp. 405–418.
31. Longuet-Higgins, M.S.; Stewart, R.W. A note on Wave setup. *J. Mar. Res.* **1963**, *21*, 4–10.
32. Mase, H. Random wave runup height on gentle slope. *J. Waterw. Port Coast. Ocean. Eng.* **1989**, *115*, 649–661. [CrossRef]
33. Mentaschi, L.; Besio, G.; Cassola, F.; Mazzino, A. Performance evaluation of WavewatchIII in the Mediterranean Sea. *Ocean Modelling* **2015**, *90*, 82–94. [CrossRef]
34. Weggel, J.R. Maximum breaker height. *J. Waterw. Harb. Coast. Eng. Div.* **1972**, *98*, 529–548. [CrossRef]